

Article

Chiral Dy(III) Fluorescent Single-Molecule Magnet Based on an Achiral Flexible Ligand

Min Zeng¹, Lin Miao¹, Xue-Ru Wu¹, Cai-Ming Liu²  and Hui-Zhong Kou^{1,*} ¹ Department of Chemistry, Tsinghua University, Beijing 100084, China² Beijing National Laboratory for Molecular Sciences, Centre for Molecular Science, Institute of Chemistry, Chinese Academy of Sciences, Beijing 100190, China

* Correspondence: kouhz@mail.tsinghua.edu.cn

Abstract: A novel multi-channel barcode module was developed by using chiral co-crystals which contain field-induced SMM behavior and different emission bands. The chiral co-crystals [Zn(H₂L)Dy(DBM)₂]₄(ClO₄)₄·9CH₃OH·H₂O (**1a**) and [Zn(H₂L)Dy(DBM)₂]₄(ClO₄)₄·8CH₃OH·0.5H₂O (**1b**) (H₄L = 2,2'-[1,2-ethanediylbis(hydroxyethylimino)methylene]]bis[6-methoxy-4-methyl-phenol], HDBM = dibenzoylmethane) were obtained through one-pot reaction of Zn^{II} and Dy^{III} with the achiral ligands H₄L and HDBM. X-ray single crystal diffraction and CD spectroscopy confirmed that they are enantiomers crystallized in *P*₄₃ (**1a**) and *P*₄₁ (**1b**), both consisting of two Δ-[Zn(H₂L)Dy(DBM)₂]⁺ cations, two Λ-[Zn(H₂L)Dy(DBM)₂]⁺ cations and four (ClO₄)⁻ anions. The presence of Dy^{III} ions endow them with the property of field-induced slow magnetic relaxation. The relatively low energy barrier of 35.0(9) K for complex **1** may be due to the poor axiality of the ligand field caused by the long Dy-O_{phenoxy} bond lengths and the small O_{phenoxy}-Dy-O_{phenoxy} bond angles. Moreover, when the organic ligands H₄L (λ_{ex} = 350 nm) and Dy^{III} (λ_{ex} = 420 nm) are excited, different emission spectra are observed.



Citation: Zeng, M.; Miao, L.; Wu, X.-R.; Liu, C.-M.; Kou, H.-Z. Chiral Dy(III) Fluorescent Single-Molecule Magnet Based on an Achiral Flexible Ligand. *Magnetochemistry* **2022**, *8*, 166. <https://doi.org/10.3390/magnetochemistry8120166>

Academic Editors: Zhao-Yang Li and Quan-Wen Li

Received: 29 October 2022

Accepted: 21 November 2022

Published: 23 November 2022

Publisher's Note: MDPI stays neutral with regard to jurisdictional claims in published maps and institutional affiliations.



Copyright: © 2022 by the authors. Licensee MDPI, Basel, Switzerland. This article is an open access article distributed under the terms and conditions of the Creative Commons Attribution (CC BY) license (<https://creativecommons.org/licenses/by/4.0/>).

Keywords: flexible ligand; chiral co-crystal; single-molecule magnet; fluorescence; dysprosium

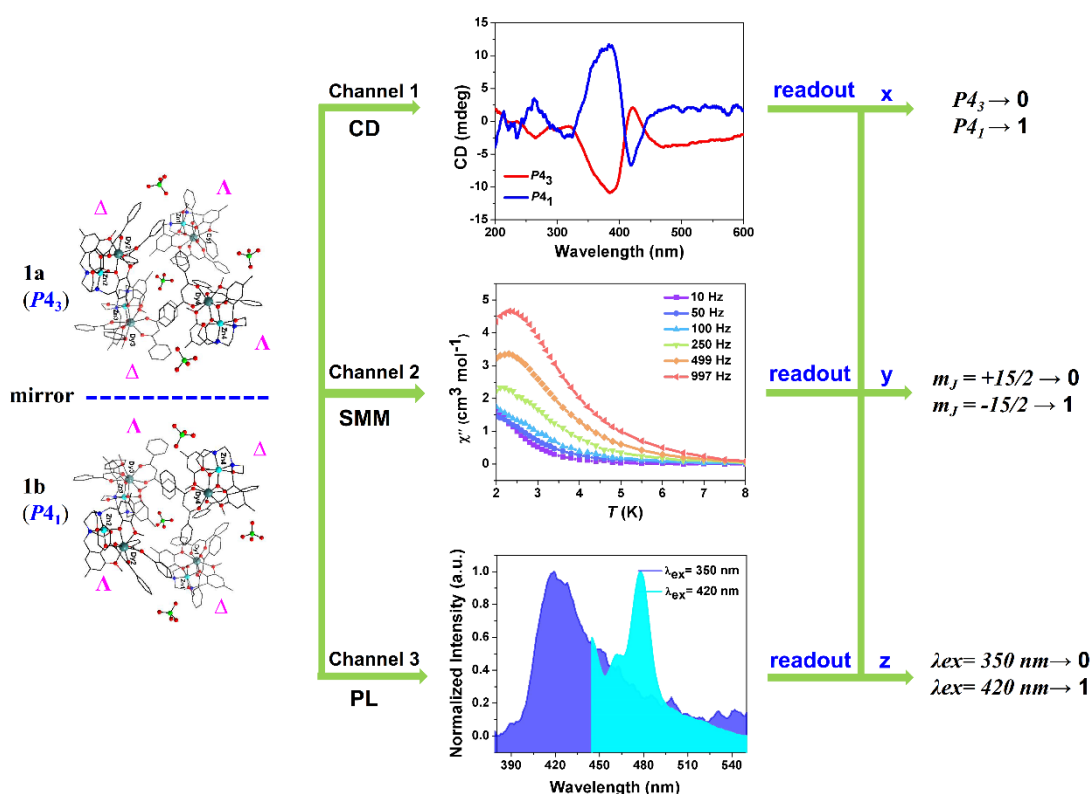
1. Introduction

Barcodes, as an important medium for information storage, play a crucial role in transportation, education and national security [1–3]. The ever-increasing demand for information security calls for higher requirements on the coding ability of barcodes [4–7]. Combining multiple storage technologies to construct multi-channel barcode modules is an effective strategy to improve information storage capability [8]. Circular dichroism (CD) is the differential absorption of left- and right-handed chiral species, which is related to the ground states of the chiral structures [9,10], and has important applications in optical storage. Single-molecule magnets (SMMs) are special metal-organic complexes that can switch between “0” and “1” in the direction of magnetic field at a certain temperature, which can be used for magnetic storage and have a larger storage capacity compared with conventional magnets [11–16]. Therefore, chiral species combining CD and SMM behavior form a family of potential two-channel magneto-optical storage materials. In recent years, luminescent materials with multiple emission bands have been widely used in barcodes [8,17–22]. For example, Zhao et al. designed multicolor photonic barcodes using 1D Ln-MOF multi-block heterostructures [20]. Su et al. established a dual-channel barcode module by Pr^{III}-MOF crystals [21].

Based on the above considerations, we are interested in designing a three-channel barcode module with multiple emission bands through chiral SMMs. According to our previous report, a chiral Co^{II}Dy^{III} SMM with the energy gap of 89.9 K was obtained based on the achiral ligands 2,2'-[1,2-ethanediylbis(hydroxyethylimino)methylene]]bis[6-methoxy-4-methyl-phenol] (H₄L) and dibenzoylmethane (HDBM) [23]. H₄L is a luminescent ligand

and the Dy^{III} ion can emit light in the visible range. In order to generate and maintain multiple emission bands, the Co^{III} ion is replaced with the Zn^{II} ion in this paper.

Herein, we propose a novel multi-channel barcode module based on a chiral SMM which contains two different emission bands upon excitation of the metal ion and organic ligand. As shown in Scheme 1, the as-prepared chiral co-crystals [Zn(H₂L)Dy(DBM)₂]₄(ClO₄)₄·9CH₃OH·H₂O (**1a**) and [Zn(H₂L)Dy(DBM)₂]₄(ClO₄)₄·8CH₃OH·0.5H₂O (**1b**) are enantiomers crystallized in *P*4₃ (**1a**) and *P*4₁ (**1b**) with mirror-symmetric CD spectra and allow for the definition of one channel of the barcode. Moreover, the presence of Dy^{III} ions gives the kryptoracemate (hidden racemate) [24] complex **1** the property of field-induced SMM behavior with the relatively low energy barrier of 35.0(9) K, which can also be defined as the other one channel of the barcode. Furthermore, complex **1** emits different emission spectra upon excitation of the organic ligand H₄L (λ_{ex} = 350 nm) and the metal ion Dy^{III} (λ_{ex} = 420 nm), further increasing the barcoding channel. This study not only provides some valuable information for the design of novel chiral complexes, but also opens up a new way to construct multi-channel barcodes.



Scheme 1. Schematic representation of using chiral co-crystals as a multi-channel barcode module.

2. Results

2.1. Crystal Structures

H₄L, HDBM, Zn(ClO₄)₂·6H₂O, Dy(ClO₄)₃·6H₂O and triethylamine was dissolved in a MeOH/MeCN mixture, and the resultant solution was slowly evaporated at room temperature, giving rise to the concurrent crystallization of [Zn(H₂L)Dy(DBM)₂]₄(ClO₄)₄·9CH₃OH·H₂O **1a** or [Zn(H₂L)Dy(DBM)₂]₄(ClO₄)₄·8CH₃OH·0.5H₂O **1b**. The crystallographic data (Table 1) show that (**1a**) and (**1b**) crystallize in the chiral space groups *P*4₃ and *P*4₁ with the Flack factor of −0.0025(14) and 0.0012(16), respectively, indicating that **1a** and **1b** are chiral (hidden racemate). The powder X-ray diffraction (PXRD) patterns of the products are in good agreement with the simulated diffraction patterns of **1a** and **1b** (Figure S1), which further indicates that there is no other impurity phase. The calculated formulas of **1a** or **1b** were consistent with the results of CHN element analysis for the kryptoracemates. As shown in Figure 1, the achiral flexible ligand H₄L was synthesized by the reaction of

2-methoxy-4-methylphenol, *N,N'*-Bis(2-hydroxyethyl)ethylenediamine and formaldehyde through a Mannich condensation reaction [25]. The detailed self-assembly process of complexes **1a** and **1b** is as follows: Firstly, H₄L chelates with Zn²⁺ through two N atoms, two O_{hydroxy} atoms and two O_{phenoxy} atoms to form Zn(H₂L); secondly, Zn(H₂L) is connected to Dy³⁺ through two O_{phenoxy} atoms and two O_{ether} atoms, and then the generated [Zn(H₂L)Dy]³⁺ moiety is linked to two DBM⁻ to form a [Zn(H₂L)Dy(DBM)₂]⁺ cation with Δ- or Λ-configuration around Dy(III); finally, four [Zn(H₂L)Dy(DBM)₂]⁺ cations and four ClO₄⁻ anions self-assemble into mirror-symmetric **1a** or **1b**. The existence of ClO₄⁻ anion was confirmed by the peak at ~1087 cm⁻¹ in the IR spectrum.

Table 1. Crystal data for complexes **1a** and **1b**.

Complexes	1a	1b
formula	C ₂₂₅ H ₂₆₂ Cl ₄ Dy ₄ N ₈ O ₆₆ Zn ₄	C ₂₂₄ H ₂₅₇ Cl ₄ Dy ₄ N ₈ O _{64.5} Zn ₄
formula weight	5187.95	5146.90
<i>T</i> /K	173(2)	173(2)
crystal system	tetragonal	tetragonal
space group	<i>P</i> 4 ₃	<i>P</i> 4 ₁
<i>a</i> , <i>b</i> /Å	29.7479(2)	29.7491(2)
<i>c</i> /Å	25.3023(3)	25.3017(2)
<i>α</i> , <i>β</i> , <i>γ</i> /°	90	90
<i>V</i> /Å ³	22,391.0(4)	22,392.2(3)
<i>Z</i>	4	4
ρ_{calc} /g·cm ⁻³	1.539	1.527
μ /mm ⁻¹	8.583	8.562
F(000)	10,192	10,500
data/restraints/parameters	29,484/102/2724	34,446/103/2666
GOF on <i>F</i> ²	1.019	1.013
<i>R</i> _{int}	0.0253	0.0253
<i>R</i> ₁ , <i>wR</i> ₂ [<i>I</i> ≥ 2σ(<i>I</i>)]	0.0338, 0.0860	0.0420, 0.1092
<i>R</i> ₁ , <i>wR</i> ₂ (all data)	0.0357, 0.0872	0.0442, 0.1111
Flack parameter	−0.0025(14)	0.0012(16)
CCDC	2,209,058	2,209,059

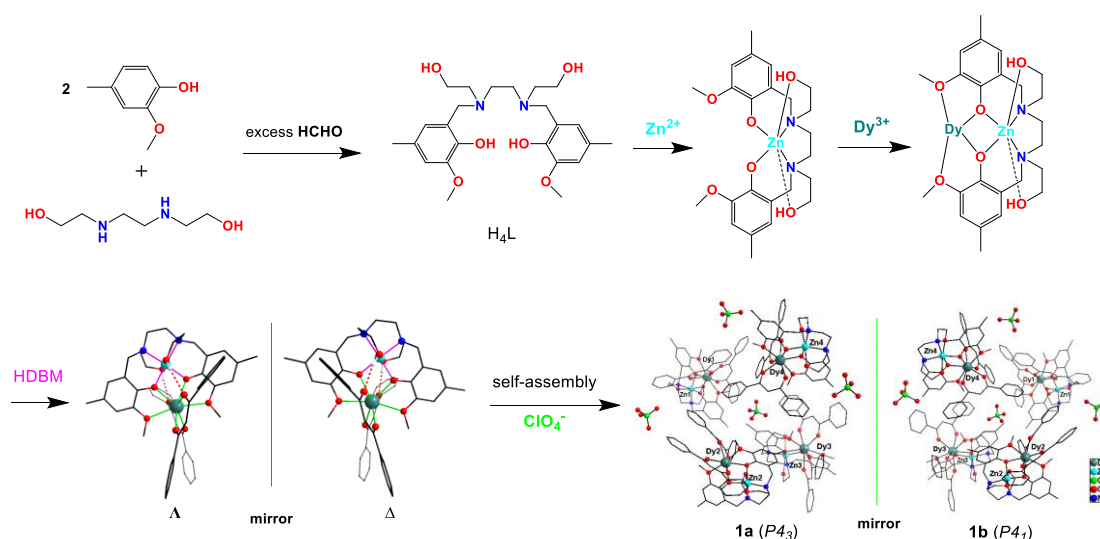


Figure 1. The formation process of complexes **1a** (*P*4₃) and **1b** (*P*4₁).

The solid-state CD spectra of **1a** and **1b** were measured with two individual single crystals by several attempts because the crystal shapes of **1a** and **1b** are indistinguishable. Two opposite CD signals are successfully obtained, as shown in Figure 2. For **1a**, negative CD signal is detected at 265 and 385 nm, and positive CD signal is detected at 420 nm. In

contrast, the CD signal for **1b** is positive at 265 and 385 nm, and negative at 420 nm. The near-perfect mirror-image CD spectra in the range of 200–600 nm confirm the optical purity of **1a** and **1b**. The UV-vis spectra of complexes **1a** and **1b** in the solid state have obvious broad absorption in the range of 200–470 nm, which is basically consistent with the CD peaks.

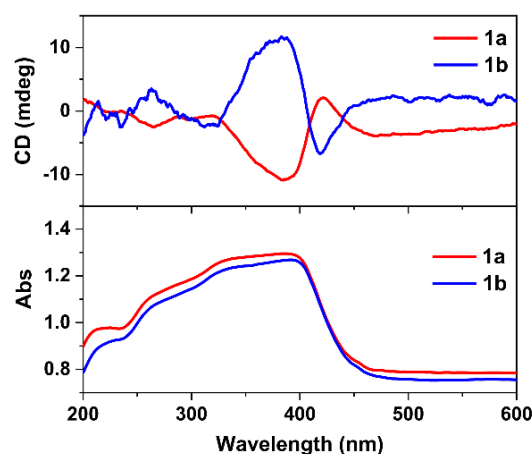


Figure 2. Solid-state CD spectra of **1a** and **1b** (KCl pellets).

Chiral co-crystals formed from the same number of Δ -configurations and Λ -configurations are rare. Complexes **1a** and **1b** are the first reported enantiomers which consist of two Δ -configurations and two Λ -configurations. As shown in Figure 3, for **1a**, Zn1-Dy1 and Zn4-Dy4 are of Λ -configurations, Zn2-Dy2 and Zn3-Dy3 are of Δ -configurations and the Δ - and Λ -ZnDy moieties are diastereomers. In contrast, for **1b**, Zn1-Dy1 and Zn4-Dy4 are Δ -configurations, and Zn2-Dy2 and Zn3-Dy3 are Λ -configurations, and similarly the Δ - and Λ -ZnDy moieties are diastereomers. The Δ - and Λ -ZnDy moieties in **1a** and **1b** are enantiomers (Figure 3). Here, only the crystal structure of Zn1-Dy1 in **1a** is selected as the example to be described. Specifically, two O_{phenoxy} atoms and two N atoms of H_2L^{2-} occupy the equatorial position of octahedral Zn atom with the Zn- O_{phenoxy} bond distances of 2.005(4) Å and the Zn-N bond distances of 2.088(5) and 2.096(5) Å. Two O_{hydroxy} atoms of H_2L^{2-} are situated at the axial position with the $O_{\text{hydroxy}}\text{-Zn-}O_{\text{hydroxy}}$ angle of 172.55° and Zn- O_{hydroxy} bond lengths of 2.239(4) and 2.290(5) Å. The Dy atom is eight-coordinate with two O_{phenoxy} atoms and two O_{ether} atoms from H_2L^{2-} , and four O_{carbonyl} atoms from two BDM^- . The Dy- O_{ether} bond distances are 2.468(4) and 2.497(4) Å, and the Dy- O_{carbonyl} bond distances of 2.266(4)–2.394(4) Å are within the normal range [26,27]. The Dy- O_{phenoxy} bond distances are 2.307(4) and 2.268(4) Å, and the $O_{\text{phenoxy}}\text{-Dy-}O_{\text{phenoxy}}$ bond angle is 71.48(13)°. The coordination geometry of Dy1 in complex **1a** calculated by SHAPE software is close to D_{4d} and D_{2d} , and the deviation parameters are 1.674 and 1.615 (Table S1), respectively. Zn and Dy atoms are connected by two O_{phenoxy} atoms with a Zn1-Dy1 distance of 3.350 Å. H_2L^{2-} and BDM^- are connected through strong intramolecular hydrogen bond with $O_{\text{hydroxy}}\text{-H-}O_{\text{carbonyl}}$ angles of 125.7 and 160.2°, and $O_{\text{hydroxy}}\text{-}O_{\text{carbonyl}}$ distances of 2.740 and 2.795 Å.

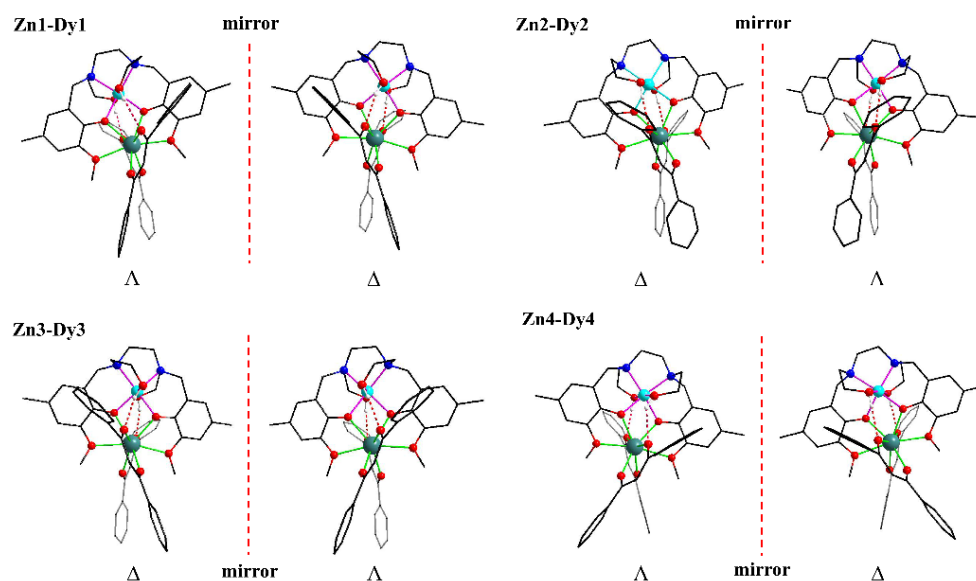


Figure 3. Coordination environments of Zn1-Dy1, Zn2-Dy2, Zn3-Dy3 and Zn4-Dy4 in complexes **1a** (left) and **1b** (right). Some hydrogen atoms are omitted for clarity.

2.2. Magnetic Properties

Since complexes **1a** and **1b** are mirror-related kryptoracemates with similar magnetic properties, only the magnetic properties of complex **1** (a mixture of **1a** and **1b**) are measured. As shown in Figure 4, the room temperature $\chi_M T$ value for complex **1** is $56.98 \text{ cm}^3 \text{ K mol}^{-1}$, which is consistent with the theoretical value of $56.68 \text{ cm}^3 \text{ K mol}^{-1}$ for four Dy^{III} ions ($g = 4/3$, ${}^6\text{H}_{15/2}$) and four diamagnetic Zn^{II} ions. Upon decreasing the temperature, the $\chi_M T$ value was almost unchanged in the range of 300–100 K, and slowly decreased to the lowest value of $44.92 \text{ cm}^3 \text{ K mol}^{-1}$ in the range of 100–8 K. The plot of $1/\chi_M$ vs. T in the range of 8–300 K conforms to the Curie–Weiss law with $\theta = -4.54 \text{ K}$ (Figure S2), which is due to the existence of crystal-field splitting of $\text{Dy}(\text{III})$ in complex **1**. However, as the temperature continues to decrease to 2 K, the $\chi_M T$ value slightly increases to $46.38 \text{ cm}^3 \text{ K mol}^{-1}$, which may be attributed to the intermolecular ferromagnetic interaction. The M – H curve of complex **1** at 2 K rapidly increases from 0 to $20.38 N\beta$, and then slowly increases to the maximum value of $25.26 N\beta$, which is much lower than the theoretical saturation value of $40 N\beta$ for four Dy^{III} ions due to the magnetic anisotropy of the Dy^{III} ion. In addition, the M – H curves at 2, 3, 4, 5 and 6 K are not overlapped, which again confirms the existence of magnetic anisotropy [28].

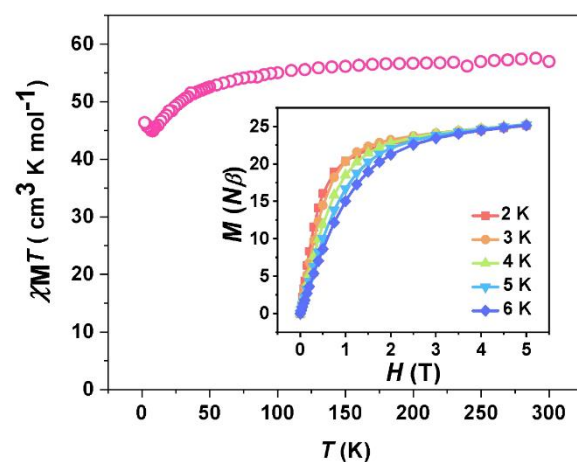


Figure 4. Temperature dependence of magnetic susceptibility for complex **1** ($H_{\text{dc}} = 1000 \text{ Oe}$). Inset: Field dependence of magnetization for complex **1** at 2, 3, 4, 5 and 6 K.

In order to study the dynamic magnetic relaxation of complex **1**, the temperature dependence of *ac* magnetic susceptibility was investigated in an oscillating field of 2.5 Oe. As shown in Figure S3, the plot of χ'' versus H for complex **1** at 997 Hz shows that 600 Oe is the best *dc* field, while the plot of χ'' vs. T shows no peak at 600 Oe. Then, the *dc* fields of 0, 1500 and 2000 Oe were selected, respectively, to obtain the plots of χ'' vs. T (Figure S4). The plot of χ'' vs. T at 1500 Oe shows a more obvious peak than that of a 2000 Oe *dc* field, therefore, a *dc* field of 1500 Oe was applied to suppress the quantum tunnelling of magnetization (QTM). Under the *dc* field of 1500 Oe, both the in-phase χ' and the out-of-phase χ'' exhibit obvious frequency dependence in the range of 2–8 K (Figures S5 and 5a), which indicates the field-induced slow magnetic relaxation of complex **1**. As shown in Figure 5b, the scatter plot of $\ln\tau$ vs. T^{-1} was derived from the peak temperature values of the χ'' vs. T plots at the frequencies of 100, 250, 499 and 997 Hz, which was fitted according to the Arrhenius' law of $\ln\tau = \ln\tau_0 + U_{\text{eff}}/kT$ (τ_0 is the relaxation time, U_{eff}/k is the relaxation energy barrier), resulting in $\tau_0 = 3.9(4) \times 10^{-11}$ s and $U_{\text{eff}}/k = 35.0(9)$ K. A τ_0 value within the range of 10^{-12} – 10^{-6} s further indicates that complex **1** is a typical field-induced SMM. The relatively low energy barrier may be due to the poor axiality of the ligand field: the Dy–O_{phenoxy} bond length is in the range of 2.268–2.321(4) Å, while the O_{phenoxy}–Dy–O_{phenoxy} bond angle is in the range of 70.1248(13)–72.17(14)°, which is far away from the perfect 180°. As shown in Figure S6, the Cole–Cole plots show a characteristic double magnetic relaxation for complex **1**, which can be fitted to obtain $\alpha_1 = 0.163$ – 0.251 and $\alpha_2 = 0.299$ – 0.348 (Table S2), which correspond to two crystallographically independent Dy^{III} ions [29]. Of course, theoretical calculations could provide more accurate information on the relaxation mechanism of such ZnDy SMMs, which deserves future investigations.

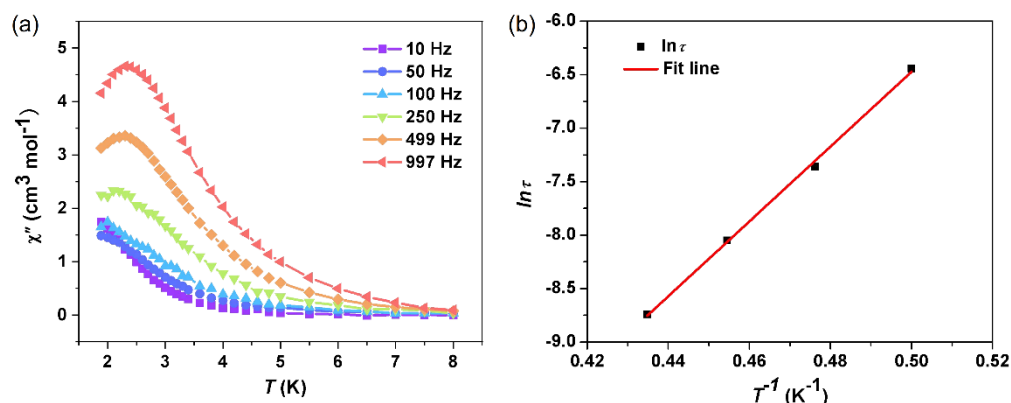


Figure 5. (a) Temperature dependent χ'' *ac* susceptibility for complex **1** ($H_{\text{dc}} = 1500$ Oe); (b) the $\ln(\tau)$ vs. T^{-1} plots based on the Arrhenius relationship for complex **1**.

2.3. Luminescent Properties

The luminescent properties of complex **1** in MeCN were investigated, as shown in Figure 6a. Upon excitation at 350 nm, complex **1** exhibits a broad band similar to H_4L , which can be attributed to the characteristic peak of the H_2L^{2-} moiety in **1**. However, the band appears at 420 nm for complex **1** and 402 nm for H_4L , and the emissive intensity of complex **1** is nearly 85 times weaker than that of H_4L . The weakened intensity may be due to the inner-filter effect (IFE) in complex **1** in the presence of the overlap between the emission and the visible absorption at ca. 402 nm (Figure 2). As shown in Figure 6b, the excitation spectrum of complex **1** was recorded by monitoring the characteristic emission band of Dy^{III} ions at 478 nm. The peaks at 402 and 420 nm originate from the intra-ligand $\pi \rightarrow \pi^*$ transitions, while the peak at 432 nm is due to the $f \rightarrow f^*$ transition of the Dy^{III} ion from the ${}^6\text{H}_{15/2}$ ground state to the ${}^4\text{G}_{11/2}$ excited state [30]. Therefore, the emission spectrum of complex **1** was recorded upon the excitation of 420 nm. There are two peaks at 462 and 478 nm, corresponding to the ${}^4\text{I}_{15/2} \rightarrow {}^6\text{H}_{15/2}$ and ${}^4\text{F}_{9/2} \rightarrow {}^6\text{H}_{15/2}$ transitions of Dy^{III} [31,32].

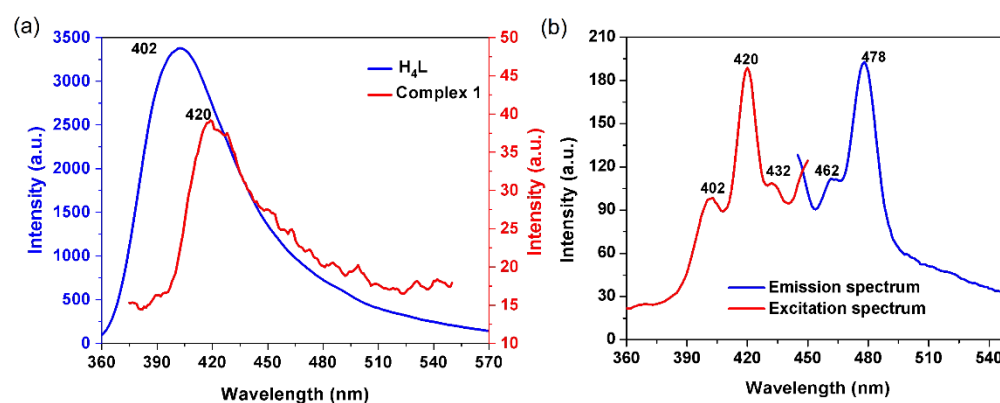


Figure 6. (a) Emission spectra of H₄L and complex 1 in MeCN with $\lambda_{\text{ex}} = 350$ nm; (b) excitation ($\lambda_{\text{em}} = 478$ nm) and emission spectra ($\lambda_{\text{ex}} = 420$ nm) for complex 1 in MeCN.

3. Materials and Methods

3.1. Materials

Methanol (MeOH), acetonitrile (MeCN), 2-methoxy-4-methylphenol, *N,N'*-Bis(2-hydroxyethyl)ethylenediamine, formaldehyde, dibenzoylmethane (HDBM), Zn(ClO₄)₂·6H₂O, Dy(ClO₄)₃·6H₂O and triethylamine were purchased from commercial sources and used without further purification.

3.2. The Preparation of Complex 1

H₄L was prepared according to the method we reported previously [23]. The mixture of H₄L (45 mg, 0.1 mmol), HDBM (45 mg, 0.2 mmol), Zn(ClO₄)₂·6H₂O (37 mg, 0.1 mmol) and 96 μ L Dy(ClO₄)₃·6H₂O aqueous solution (50%, 0.1 mmol) was dissolved in acetonitrile (5 mL) and methanol (10 mL). Then, triethylamine (100 μ L) was slowly added and stirred for 3 min. Subsequently, the above solution was filtered and slowly evaporated without disturbance at room temperature. Colorless needle crystals of complex 1 were obtained after 2 days. Yield: about 74%. Two types of crystal structures were obtained by single crystal X-ray diffraction analysis on several randomly selected single crystals. Anal. calcd (%) for C₂₂₅H₂₆₂Cl₄Dy₄N₈O₆₆Zn₄ (**1a**): C, 52.09; H, 5.09; and N, 2.16. Anal. calcd (%) for C₂₂₄H₂₅₇Cl₄Dy₄N₈O_{64.5}Zn₄ (**1b**): C, 52.27; H, 5.03; and N, 2.18. Found for **1a** + **1b**: C, 52.9; H, 5.0; and N, 2.4. Main IR peaks (KBr, cm⁻¹): 1593 (s), 1544 (vs), 1521 (vs), 1481 (vs), 1452 (m), 1390 (vs), 1315 (m), 1250 (m), 1087 (vs), 816 (m), 728 (m), 694 (w), and 617 (m).

3.3. Physical Measurements

IR spectra was recorded on a Beijing Rayleigh WQF-510A FTIR spectrometer. CHN element analysis was tested on a thermal Flash EA 1112 elemental analyzer. Powder X-ray diffraction (PXRD) was measured on a Rigaku D/max 2500 diffractometer. Circular dichroism (CD) spectra were measured on a JASCO J-1500 spectrometer. Luminescence spectra were tested on a Hitachi F-7000 fluorescence spectrometer. Magnetic measurements were carried on a SQUID MPMS-XL5 magnetometer, and the Pascal's constants were used to correct the diamagnetism. Single-crystal X-ray diffraction was performed on a Rigaku Super Nova diffractometer. The crystal structures were solved and refined by OLEX-2 software. To resolve the severe disorder of the lattice solvent molecules of complexes **1a** and **1b**, the SQUEEZE function of PLATON software was applied. For complex **1a**, 104 electrons in the hole of 509 \AA^3 correspond to 5CH₃OH and 1H₂O for each formula (100 electrons). For **1b**, 133 electrons in the hole of 822 \AA^3 correspond to 7CH₃OH and 0.5H₂O for each formula (131 electrons).

4. Conclusions

In summary, we have developed a novel multi-channel barcode module based on chiral co-crystal complexes **1a** and **1b**, which contain field-induced SMM behavior and different

emission bands. Complexes **1a** and **1b** are the first chiral kryptoracemate complexes composed of four independent binuclear Zn-Dy groups, two of which are Δ -configuration and two are Λ -configuration. These two chiral complexes have mirror-related structures and mirror-symmetric CD spectra. Complex **1** shows field-induced SMM behavior with an energy barrier of 35.0(9) K. Moreover, luminescence measurements show that complex **1** exhibits different luminescence emissions under the excitation of UV or visible light. The present work provides some valuable information for the construction of novel chiral complexes from achiral ligands, and describes a new strategy for creating multi-channel barcode modules for high-density information storage.

Supplementary Materials: The following are available online at <https://www.mdpi.com/article/10.3390/magnetochemistry8120166/s1>, Figure S1: PXRD patterns for complex **1**. Figure S2: Plot of the $1/\chi_M$ versus T for **1**. The red solid line represents the linear fit of the data. Figure S3: (left) Plot of χ'' versus H for complex **1** at 997 Hz and (right) plot of χ'' versus T for complex **1** at 997 Hz under 600 Oe dc field. Figure S4: Plots of χ'' versus T for complex **1** at 997 Hz under 0, 1500 and 2000 Oe dc field, respectively. Figure S5: Plots of temperature dependent χ' ac susceptibility for complex **1** ($H_{dc} = 1500$ Oe). Figure S6: Cole-Cole curves at 1.9–2.3 K ($H_{dc} = 1500$ Oe, $H_{ac} = 2.5$ Oe). Table S1: The coordination geometry of Dy1 in **1a** calculated by SHAPE software. Table S2: Cole-Cole curve fitting parameters for complex **1**.

Author Contributions: All authors participated in the writing and editing of the article, M.Z., L.M., X.-R.W., C.-M.L. and H.-Z.K. All authors have read and agreed to the published version of the manuscript.

Funding: This research was funded by the National Natural Science Foundation of China, grant numbers 21971142 and 21771115.

Informed Consent Statement: Not applicable.

Conflicts of Interest: The authors declare no conflict of interest.

References

1. White, K.A.; Chengelis, D.A.; Gogick, K.A.; Stehman, J.; Rosi, N.L.; Petoud, S. Near-Infrared Luminescent Lanthanide MOF Barcodes. *J. Am. Chem. Soc.* **2009**, *131*, 18069–18071. [[CrossRef](#)]
2. Zhang, Y.; Zhang, L.; Deng, R.; Tian, J.; Zong, Y.; Jin, D.; Liu, X. Multicolor barcoding in a single upconversion crystal. *J. Am. Chem. Soc.* **2014**, *136*, 4893–4896. [[CrossRef](#)] [[PubMed](#)]
3. Lu, Y.; Yan, B. Luminescent lanthanide barcodes based on postsynthetic modified nanoscale metal–organic frameworks. *J. Mater. Chem. C* **2014**, *2*, 7411–7416. [[CrossRef](#)]
4. Zhao, Y.; Shum, H.C.; Chen, H.; Adams, L.L.; Gu, Z.; Weitz, D.A. Microfluidic generation of multifunctional quantum dot barcode particles. *J. Am. Chem. Soc.* **2011**, *133*, 8790–8793. [[CrossRef](#)] [[PubMed](#)]
5. Zhang, F.; Haushalter, R.C.; Haushalter, R.W.; Shi, Y.; Zhang, Y.; Ding, K.; Zhao, D.; Stucky, G.D. Rare-earth upconverting nanobarcodes for multiplexed biological detection. *Small* **2011**, *7*, 1972–1976. [[CrossRef](#)] [[PubMed](#)]
6. Pan, M.; Zhu, Y.X.; Wu, K.; Chen, L.; Hou, Y.J.; Yin, S.Y.; Wang, H.P.; Fan, Y.N.; Su, C.Y. Epitaxial Growth of Hetero-Ln-MOF Hierarchical Single Crystals for Domain- and Orientation-Controlled Multicolor Luminescence 3D Coding Capability. *Angew. Chem. Int. Ed. Engl.* **2017**, *56*, 14582–14586. [[CrossRef](#)] [[PubMed](#)]
7. Chen, C.; Zhang, P.; Gao, G.; Gao, D.; Yang, Y.; Liu, H.; Wang, Y.; Gong, P.; Cai, L. Near-infrared-emitting two-dimensional codes based on lattice-strained core/(doped) shell quantum dots with long fluorescence lifetime. *Adv. Mater.* **2014**, *26*, 6313–6317. [[CrossRef](#)]
8. Shikha, S.; Salafi, T.; Cheng, J.; Zhang, Y. Versatile design and synthesis of nano-barcodes. *Chem. Soc. Rev.* **2017**, *46*, 7054–7093. [[CrossRef](#)]
9. Ishii, A.; Miyasaka, T. Direct detection of circular polarized light in helical 1D perovskite-based photodiode. *Sci. Adv.* **2020**, *6*, eabd3274. [[CrossRef](#)]
10. Zeng, M.; Ren, A.; Wu, W.; Zhao, Y.; Zhan, C.; Yao, J. Lanthanide MOFs for inducing molecular chirality of achiral stilbazolium with strong circularly polarized luminescence and efficient energy transfer for color tuning. *Chem. Sci.* **2020**, *11*, 9154–9161. [[CrossRef](#)]
11. Lu, J.; Guo, M.; Tang, J. Recent Developments in Lanthanide Single-Molecule Magnets. *Chem.-Asian J.* **2017**, *12*, 2772–2779. [[CrossRef](#)] [[PubMed](#)]
12. Marin, R.; Brunet, G.; Murugesu, M. Shining New Light on Multifunctional Lanthanide Single-Molecule Magnets. *Angew. Chem.-Int. Ed.* **2020**, *60*, 1728–1746. [[CrossRef](#)]

13. Meng, Y.-S.; Jiang, S.-D.; Wang, B.-W.; Gao, S. Understanding the Magnetic Anisotropy toward Single-Ion Magnets. *Acc. Chem. Res.* **2016**, *49*, 2381–2389. [[CrossRef](#)] [[PubMed](#)]
14. Zhu, Z.; Zhao, C.; Feng, T.; Liu, X.; Ying, X.; Li, X.-L.; Zhang, Y.-Q.; Tang, J. Air-Stable Chiral Single-Molecule Magnets with Record Anisotropy Barrier Exceeding 1800 K. *J. Am. Chem. Soc.* **2021**, *143*, 10077–10082. [[CrossRef](#)] [[PubMed](#)]
15. Chen, Y.-C.; Liu, J.-L.; Ungur, L.; Liu, J.; Li, Q.-W.; Wang, L.-F.; Ni, Z.-P.; Chibotaru, L.F.; Chen, X.-M.; Tong, M.-L. Symmetry-Supported Magnetic Blocking at 20 K in Pentagonal Bipyramidal Dy(III) Single-Ion Magnets. *J. Am. Chem. Soc.* **2016**, *138*, 2829–2837. [[CrossRef](#)] [[PubMed](#)]
16. Li, Z.-H.; Zhai, Y.-Q.; Chen, W.-P.; Ding, Y.-S.; Zheng, Y.-Z. Air-Stable Hexagonal Bipyramidal Dysprosium(III) Single-Ion Magnets with Nearly Perfect D-6h Local Symmetry. *Chem.-A Eur. J.* **2019**, *25*, 16219–16224. [[CrossRef](#)]
17. Yang, Q.Y.; Pan, M.; Wei, S.C.; Li, K.; Du, B.B.; Su, C.Y. Linear Dependence of Photoluminescence in Mixed Ln-MOFs for Color Tunability and Barcode Application. *Inorg. Chem.* **2015**, *54*, 5707–5716. [[CrossRef](#)]
18. Zhou, Y.; Yan, B. Ratiometric multiplexed barcodes based on luminescent metal-organic framework films. *J. Mater. Chem. C* **2015**, *3*, 8413–8418. [[CrossRef](#)]
19. Gao, M.L.; Wang, W.J.; Liu, L.; Han, Z.B.; Wei, N.; Cao, X.M.; Yuan, D.Q. Microporous Hexanuclear Ln(III) Cluster-Based Metal-Organic Frameworks: Color Tunability for Barcode Application and Selective Removal of Methylene Blue. *Inorg. Chem.* **2017**, *56*, 511–517. [[CrossRef](#)]
20. Yao, Y.; Gao, Z.; Lv, Y.; Lin, X.; Liu, Y.; Du, Y.; Hu, F.; Zhao, Y.S. Heteroepitaxial Growth of Multiblock Ln-MOF Microrods for Photonic Barcodes. *Angew. Chem.-Int. Ed.* **2019**, *58*, 13803–13807. [[CrossRef](#)]
21. Du, B.B.; Zhu, Y.X.; Pan, M.; Yue, M.Q.; Hou, Y.J.; Wu, K.; Zhang, L.Y.; Chen, L.; Yin, S.Y.; Fan, Y.N.; et al. Direct white-light and a dual-channel barcode module from Pr(III)-MOF crystals. *Chem. Commun. (Camb.)* **2015**, *51*, 12533–12536. [[CrossRef](#)] [[PubMed](#)]
22. Nguyen, H.Q.; Baxter, B.C.; Brower, K.; Diaz-Botia, C.A.; DeRisi, J.L.; Fordyce, P.M.; Thorn, K.S. Programmable Microfluidic Synthesis of Over One Thousand Uniquely Identifiable Spectral Codes. *Adv. Opt. Mater.* **2017**, *5*, 1600548. [[CrossRef](#)]
23. Liu, M.-J.; Yuan, J.; Wang, B.-L.; Wu, S.-T.; Zhang, Y.-Q.; Liu, C.-M.; Kou, H.-Z. Spontaneous Resolution of Chiral Co(III)Dy(III) Single-Molecule Magnet Based on an Achiral Flexible Ligand. *Cryst. Growth Des.* **2018**, *18*, 7611–7617. [[CrossRef](#)]
24. Sunatsuki, Y.; Fujita, K.; Maruyama, H.; Suzuki, T.; Ishida, H.; Kojima, M.; Glaser, R. Chiral Crystal Structure of a P₂₁2₁2₁ Kryptoracemate Iron(II) Complex with an Unsymmetric Azine Ligand and the Observation of Chiral Single Crystal Circular Dichroism. *Cryst. Growth Des.* **2014**, *14*, 3692–3695. [[CrossRef](#)]
25. Tshuva, E.Y.; Gendzeiuk, N.; Kol, M. Single-step synthesis of salans and substituted salans by Mannich condensation. *Tetrahedron Lett.* **2001**, *42*, 6405–6407. [[CrossRef](#)]
26. Zeng, M.; Zhou, Z.-Y.; Wu, X.-R.; Liu, C.-M.; Kou, H.-Z. Assembly of a Heterotrimetallic Zn₂Dy₂Ir Pentanuclear Complex toward Multifunctional Molecular Materials. *Inorg. Chem.* **2022**, *61*, 14275–14281. [[CrossRef](#)]
27. Zeng, M.; Ji, S.-Y.; Wu, X.-R.; Zhang, Y.-Q.; Liu, C.-M.; Kou, H.-Z. Magneto-optical Properties of Lanthanide(III) Metal-Organic Frameworks Based on an Iridium(III) Metalloligand. *Inorg. Chem.* **2022**, *61*, 3097–3102. [[CrossRef](#)]
28. Liu, C.-M.; Sun, R.; Hao, X.; Wang, B. Chiral Co-Crystals of (S)- or (R)-1,1'-Binaphthalene-2,2'-diol and Zn₂Dy₂ Tetranuclear Complexes Behaving as Single-Molecule Magnets. *Cryst. Growth Des.* **2021**, *21*, 4346–4353. [[CrossRef](#)]
29. Guo, Y.-N.; Xu, G.-F.; Gamez, P.; Zhao, L.; Lin, S.-Y.; Deng, R.; Tang, J.; Zhang, H.-J. Two-Step Relaxation in a Linear Tetranuclear Dysprosium(III) Aggregate Showing Single-Molecule Magnet Behavior. *J. Am. Chem. Soc.* **2010**, *132*, 8538. [[CrossRef](#)]
30. Li, L.; Qin, F.; Zhou, Y.; Zheng, Y.; Miao, J.; Zhang, Z. Photoluminescence and time-resolved luminescence of CaWO₄: Dy³⁺-phosphors. *J. Lumin.* **2020**, *224*, 117308. [[CrossRef](#)]
31. Zeng, M.; Zhan, C.; Yao, J. Novel bimetallic lanthanide metal-organic frameworks (Ln-MOFs) for colour-tuning through energy-transfer between visible and near-infrared emitting Ln³⁺ ions. *J. Mater. Chem. C* **2019**, *7*, 2751–2757. [[CrossRef](#)]
32. Cui, Y.; Yue, Y.; Qian, G.; Chen, B. Luminescent Functional Metal-Organic Frameworks. *Chem. Rev.* **2012**, *112*, 1126–1162. [[CrossRef](#)] [[PubMed](#)]